separations

MDPI

Article

Adsorption of Cr(III) by IRA-900 Resin in Sodium Phosphite and Sulfuric Acid System

Tingjie Xu [1], Dahuan Gan [1], Guowang Wei [2], Yingjie Yang [1], Qiankun Wei [2] and Chunlin He [1,3,*]

[1] Guangxi Key Laboratory of Processing for Non-Ferrous Metals and Featured Materials, Key Laboratory of High Performance Structural Materials and Thermo-Surface Processing, School of Resources, Environment and Materials, Guangxi University, Nanning 530004, China; 2415391107@st.gxu.edu.cn (T.X.)
[2] Hechi Institute of Scientific and Technical Information, Hechi 547000, China
[3] Guangxi Key Laboratory of Advanced Rare Earth Materials, Nanning 530004, China
* Correspondence: helink@gxu.edu.cn

Abstract

Chromium (Cr), a toxic heavy metal, poses significant environmental and health risks when industrial effluents containing Cr are discharged untreated. Addressing this challenge, this study developed a selective chromium removal strategy using IRA-900 resin in a sulfuric acid system with sodium phosphite (NaH_2PO_3) as a complexing agent. In the NaH_2PO_3-H_2SO_4 system, IRA-900 resin exhibited exceptional selectivity for Cr^{3+} with minimal co-adsorption of competing ions. The adsorption process followed the Langmuir isotherm model ($R^2 > 0.99$), indicating monolayer chemisorption dominated by homogeneous active sites, and achieved a maximum capacity of 103.56 $mg \cdot g^{-1}$. Characterization via XPS, FT-IR, and SEM-EDS revealed a two-step mechanism: Cr^{3+} reacts with $H_2PO_3^-$ to form an anionic complex, and then the complex undergoes electrostatic interaction and ion exchange with chloride ions (Cl^-) on the quaternary ammonium groups of the resin. The chromium-loaded resin demonstrated remarkable structural stability, resisting Cr^{3+} desorption under conventional elution conditions. This property provides a novel pathway for chromium solidification in industrial wastewater, effectively minimizing secondary pollution risks. This work advances the design of ligand-assisted ion-exchange systems for targeted heavy metal removal, offering both high selectivity and environmental compatibility in wastewater treatment.

Keywords: IRA-900 resin; sodium phosphite; Cr; adsorption

check for updates

Academic Editor: Maria Atanassova

Received: 30 August 2025
Revised: 28 September 2025
Accepted: 3 October 2025
Published: 5 October 2025

Citation: Xu, T.; Gan, D.; Wei, G.; Yang, Y.; Wei, Q.; He, C. Adsorption of Cr(III) by IRA-900 Resin in Sodium Phosphite and Sulfuric Acid System. *Separations* **2025**, *12*, 270. https://doi.org/10.3390/separations12100270

Copyright: © 2025 by the authors. Licensee MDPI, Basel, Switzerland. This article is an open access article distributed under the terms and conditions of the Creative Commons Attribution (CC BY) license (https://creativecommons.org/licenses/by/4.0/).

1. Introduction

Chromium (Cr) is a hard, gray metal, with its most common oxidation states being Cr(III) and Cr(VI) [1]. Trivalent chromium (Cr(III)) and hexavalent chromium (Cr(VI)) exhibit significant differences in their environmental behavior and toxicity [2]. Cr(III) is of low toxicity and tends to form insoluble chromium(III) hydroxide precipitates under natural conditions, thereby posing minimal ecological risk [3]. In contrast, Cr(VI) is classified as a priority pollutant by the U.S. Environmental Protection Agency due to its high toxicity, carcinogenicity, and environmental persistence [4–6]. Chronic exposure to Cr(VI) can lead to severe health effects, including acute inflammatory responses, gastrointestinal disorders, and carcinogenesis [4,7]. Notably, its ability to permeate cell membranes and bind to biomolecules, such as proteins and nucleic acids, significantly exacerbates its biological toxicity [8]. The direct discharge of chromium-containing industrial effluents, such

as tannery wastewater (which accounts for approximately 8% of China's annual tannery effluent volume of 70 million tons [9]), poses a significant threat to ecosystems. Therefore, the efficient removal of chromium from wastewater is imperative for environmental protection and resource sustainability [10].

Although the primary environmental concern often centers on Cr(VI), its reduction to Cr(III) is a well-established and common first step in industrial wastewater treatment [11,12]. However, this process converts the pollution issue from a toxic and mobile form (Cr(VI)) into a less toxic, yet still challenging, solid waste disposal problem. Conventional Cr(III) removal relies on alkaline precipitation, which generates voluminous hydrous sludge that is difficult to dewater, stabilize, and dispose of safely [13]. Such sludge presents long-term environmental risks due to the potential for re-leaching. Consequently, there is a critical and growing need for innovative technologies capable of selectively sequestering and stabilizing Cr(III) from complex wastewater streams, thereby providing a more sustainable and definitive solution following the initial Cr(VI) reduction step.

Current conventional chromium removal methodologies encompass chemical precipitation, electrochemical processes, membrane separation, solvent extraction, and adsorption techniques [14]. For instance, Jiao et al. [15] employed an acid leaching–alkali precipitation–evaporation approach to recover chromium from waste magnesia-chrome refractories. Although this method facilitates resource recovery, its multi-step nature, high energy consumption, and lack of validation for treating low-concentration chromium-containing wastewater limit its direct applicability in wastewater treatment. Yao et al. [16] achieved simultaneous removal of Cr(VI) and Cr(III) via electrolysis using a titanium (Ti) anode. Mechanistic analysis indicated that corrosion of the Ti anode produces Ti^{3+} and Ti^{2+} species, which provide electrons for the reduction in Cr(VI) to Cr(III), while continuous generation of hydroxide ions (OH^-) at the cathode promotes precipitation. Maximum removal efficiencies of 80.5% for Cr(VI) and 79.4% for total chromium were achieved within 12 h. Silva et al. [17] reported 96.5% chromium removal during electroplating of raw tannery wastewater, noting that the addition of a defoamer effectively suppressed foam formation without reducing removal efficiency. Riaz et al. [18] developed and characterized polyurethane–cellulose acetate blend membranes and evaluated their permeability and Cr(VI) rejection performance under varying pH, pressure, and salt concentration conditions. Optimal Cr(VI) removal was observed at pH 3 under an operating pressure of 0.4 MPa. Wang et al. [19] achieved efficient separation of chromium and vanadium through solvent extraction using EHEHPA–sulfate ion complexation. While this study highlights the potential of complexation for improving selectivity, its primary focus is metal separation rather than deep purification, and the solvent extraction process may involve risks of organic phase loss and secondary pollution. Similarly, Rim et al. [20] demonstrated the extraction of Cr(III) from aqueous solutions using polyoxyethylene alcohols in the presence of sodium dodecylbenzenesulfonate. Although this method provides an alternative strategy for complexation, it introduces surfactants, which increases both the complexity and cost of the system, and may potentially lead to new environmental issues.

In summary, although existing technologies each possess their own advantages, they commonly suffer from limitations such as complex processes, high energy consumption, a tendency to cause secondary pollution, and difficulties in balancing selectivity with operational simplicity. Therefore, it remains necessary to develop a novel method for chromium removal that is efficient, highly selective, environmentally friendly, and easy to operate.

Adsorption is a physicochemical separation technique that utilizes the sorption capacity of porous solid-phase adsorbents to selectively sequester and isolate target metal ions from aqueous solutions. Elabbas et al. [21] investigated the efficacy of biogenic ad-

sorbents, namely eggshell and marble powder, for removing Cr(III) from chrome tanning wastewater. Through systematic evaluation of operational parameters—including pH, adsorbent dosage, and contact time—optimal performance was achieved at pH 5.0, with adsorbent loadings of 20 $g \cdot L^{-1}$ for eggshell and 12 $g \cdot L^{-1}$ for marble powder, reaching equilibrium within 14 h and 30 min, respectively. Under these optimized conditions, near-complete Cr(III) removal (99%) was achieved for wastewater with an initial chromium concentration of 3.21 $g \cdot L^{-1}$. Fu et al. [22] advanced this field by synthesizing a Cr(III) ion-imprinted polymer (designated Cr(III)-IIP9) via a green ion-imprinting approach using amino-functionalized chitosan derivatives. The resulting material exhibited a high adsorption capacity (385.89 $mg \cdot g^{-1}$), broad pH adaptability (2.0–8.0), fast kinetics (equilibrium within 120 min), and high selectivity for Cr(III). Owing to its operational simplicity, high removal efficiency, and adaptability to diverse wastewater matrices, adsorption is widely regarded as a sustainable and cost-effective strategy for chromium remediation [23].

This study investigates the selective adsorption of Cr^{3+} by IRA-900 resin in a sulfuric acid system mediated by sodium phosphite. The introduction of sodium phosphite promotes the formation of an anionic Cr^{3+}–phosphite complex in solution, which subsequently facilitates adsorption via an ion-exchange mechanism on the resin, thereby enhancing selectivity toward Cr^{3+}. The influence of sodium phosphite concentration on adsorption selectivity was evaluated, along with the effects of sulfuric acid concentration, contact time, temperature, and initial Cr^{3+} concentration on adsorption capacity. Desorption efficiency was also assessed using seven different elution agents.

The key innovation of this approach lies in the complexation-driven adsorption process, which not only achieves a high adsorption capacity (103.56 $mg \cdot g^{-1}$) but also offers exceptional selectivity and notable resin stability. Furthermore, the strong resistance of adsorbed Cr(III) to desorption presents a novel strategy for the solidification treatment of chromium-containing wastewater, effectively reducing the risk of secondary pollution.

2. Materials and Methods

2.1. Experimental Materials

The IRA-900 resin, a macroporous styrene-divinylbenzene copolymer matrix functionalized with quaternary ammonium groups, exhibits anion exchange capabilities through electrostatic interactions with metal ions, rendering it suitable for metal ion adsorption and separation. Analytical-grade reagents utilized in this study included: $Cr_2(SO_4)_3 \cdot xH_2O$, $NiSO_4 \cdot 6H_2O$, $ZnSO_4 \cdot 7H_2O$, $Al_2(SO_4)_3 \cdot 18H_2O$, Na_2SO_4, $CoSO_4 \cdot 7H_2O$ (Guangdong Guanghua Sci-Tech Co., Ltd., Shantou, China); $CuSO_4$, $MnSO_4 \cdot H_2O$, $3CdSO_4 \cdot 8H_2O$ (Tianjin Damao Chemical Reagent Co., Ltd., Tianjin, China); $Ga_2(SO_4)_3$, $In_2(SO_4)_3$, Na_2HPO_3 and H_2SO_4, (Shanghai Macklin Biochemical Co., Ltd., Shanghai, China).

2.2. Characterization Techniques

Ion concentrations were measured by inductively coupled plasma-atomic emission spectrometry (ICPS-7510, Shimadzu Co., Tokyo, Japan). Fourier infrared spectrometry (FT-IR racer-100, Shimadzu Co., Tokyo, Japan), high-resolution X-ray photoelectron spectroscopy (XPS, Thermo ESCALAB 250XI, Thermo Fisher Scientific (China) Co., Shanghai, China), Scanning electron microscopy with energy dispersive X-ray spectrometry(SEM-EDS, Phenom Pro 800-07334, Phenom-World B.V., Eindhoven, Netherlands) were applied to reveal the adsorption mechanism.

2.3. Experimental Procedures

2.3.1. Selective Adsorption

Cr-laden industrial effluents typically contain coexisting metal ion. To systematically evaluate the influence of sodium phosphite (Na_2HPO_3) concentration on the selectivity of IRA-900 resin, simulated mixed solutions incorporating graded Na_2HPO_3 concentrations (0.01, 0.05, 0.1, 0.5, and 1 mol·L^{-1}) were formulated. The experimental parameters were maintained as follows: time = 2 h, temperature = 298 K, Liquid-solid ratio (V/m) = 10 mL/0.1 g, and H_2SO_4 concentration = 0.5 mol·L^{-1}. The concentrations of the simulated mixed solution are detailed in Table 1. The composition of the simulated mixed solution (Table 1) was designed according to the typical characteristics of chromium-containing industrial wastewater (especially tannery wastewater [9,21,24]). The high concentration of sodium (Na, 1000 mg·L^{-1}) simulates the common saline background in such effluents. The concentrations of chromium (Cr) and other heavy metal ions (e.g., Al, Zn, Cu, Ni, at 500–1500 mg·L^{-1}) were chosen with reference to values reported in previous studies on tannery and electroplating wastewater, aiming to mimic a realistic scenario with high pollution load and the presence of multiple competing ions. The selected ions cover various valences (e.g., Al^{3+}, Cr^{3+}, Cu^{2+}, Na^{+}) and chemical behaviors to rigorously evaluate the selectivity of the IRA-900 resin in a complex system. The concentrations of all coexisting metal ions are representative of industrial scenarios.

Table 1. Concentrations of the simulated mixed solution.

Element	Na	Al	Cd	Mn	Zn	In	Ga	Cu	Ni	Co	Cr
Concentration(mg·L^{-1})	1000	1000	1500	500	500	500	500	500	500	500	500

The simulated mixed solution was prepared through the following steps: First, the respective metal sulfates were accurately weighed according to the target concentrations of each metal ion shown in Table 1. Subsequently, they were dissolved in a 0.1 mol/L sulfuric acid solution under magnetic stirring. After the solution cooled to room temperature, it was diluted to the mark in a 500 mL volumetric flask and thoroughly mixed to ensure homogeneity of the solution.

2.3.2. Static Adsorption

The effects of sulfuric acid concentration (0.5, 1, 2, and 3 mol·L^{-1}), time (10–240 min), temperature (298, 308, and 318 K), and the effect of Cr (III) initial ion concentration (C_0 = 20, 100, 200, and 400 mg·L^{-1}) on the adsorption process were investigated. Metal ion concentrations were determined using an ICPS-7510 instrument. The relevant equations are as follows:

$$\text{Adsorption capacity } (Q_e):\ Q_e = \frac{(C_1 - C_2)V}{m} \quad (1)$$

$$\text{Adsorption efficiency } (E):\ E = \frac{C_1 - C_2}{C_1} \times 100\% \quad (2)$$

$$\text{Distribution coefficient } (K_d):\ K_d = \frac{(C_1 - C_2)V}{C_1 \cdot m} \quad (3)$$

where C_1 (mg·L^{-1}) is the initial concentration, C_2 (mg·L^{-1}) is the equilibrium concentration, V (L) is the liquid volume, and m (g) is the resin mass.

By altering the initial concentration of Cr^{3+} in the solution and the adsorption temperature, adsorption isotherms at different temperatures were obtained. In the sulfuric acid solution, with initial Cr^{3+} concentrations ranging from 0 to 1700 mg·L^{-1}, isothermal

adsorption experiments were conducted at 298, 308, and 318 K. The experimental data were fitted using the Langmuir (4) and Freundlich (5) isothermal models, respectively.

$$C_e/Q_e = C_e/Q_m + 1/K_L Q_m \quad (4)$$

$$lnQ_e = lnK_f + lnC_e/n \quad (5)$$

where Q_m ($mg \cdot g^{-1}$) represents the maximum adsorption capacity per gram of resin, C_e ($mg \cdot L^{-1}$) is the concentration of Cr remaining in solution at equilibrium, K_L ($L \cdot mg^{-1}$) is the Langmuir adsorption constant, and K_f ($mg^{1-n} \cdot L^n/g$) and n are Freundlich constants related to adsorption capacity.

2.3.3. Desorption Conditions

The resin utilized for desorption was derived from saturated adsorption under the following conditions: 1000 $mg \cdot L^{-1}$ Cr^{3+}, a liquid-to-solid ratio of 40 mL/0.05 g, 1 $mol \cdot L^{-1}$ Na_2HPO_3, a duration of 24 h, a temperature of 298 K, and 0.5 $mol \cdot L^{-1}$ sulfuric acid. The desorbents comprised HNO_3, H_2SO_4, HCl, NaOH, NH_4Cl, NaCl, and $NH_3 \cdot H_2O$.

$$\text{Desorption efficiency (R)}: \ R = \frac{C_1 V_1}{Q_e \cdot m} \times 100\% \quad (6)$$

where C_1 ($mg \cdot L^{-1}$) is the initial concentration, V_1 (L) is the liquid volume, Q_e ($mg \cdot g^{-1}$) is the adsorption capacity of the resin for Cr ions, and m (g) is the resin mass.

2.3.4. Speciation Profiles for Cr(III)

The morphological characteristics of Cr(III) are shown in Figure 1. In aqueous solutions, Cr(III) primarily exists in seven distinct species, the distribution of which varies with pH [25]. At pH 2, Cr^{3+} constitutes 100% of the total Cr(III) species, but it completely disappears at pH 5. Under the optimal experimental conditions (0.5 mol/L H_2SO_4 and 1 mol/L Na_2HPO_3), when the pH is 3.5, Cr(III) predominantly exists as Cr^{3+} and $CrOH^{2+}$, with Cr^{3+} being the dominant species, accounting for approximately 60% of the total Cr(III).

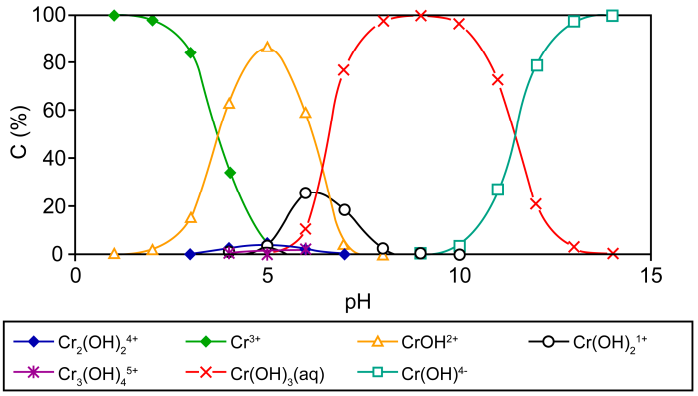


Figure 1. Speciation profiles for Cr(III).

3. Results and Discussion

3.1. Influence of Sodium Phosphite Concentration on Adsorption Selectivity

The influence of sodium phosphite concentration on the distribution coefficients and adsorption capacities of various metal ions is shown in Figure 2a,b. Under conditions of 0.5 $mol \cdot L^{-1}$ sulfuric acid without sodium phosphite, the resin exhibited negligible adsorption of Cr^{3+}. Both the distribution coefficient and adsorption capacity increased significantly with rising sodium phosphite concentration. At 1 $mol \cdot L^{-1}$ sodium phosphite, the distribution coefficient and adsorption capacity for Cr^{3+} reached 55 $dm^3 \cdot kg^{-1}$ and 27 $mg \cdot g^{-1}$, respectively. Comparative analysis indicated pronounced selectivity for Cr^{3+}

over coexisting ions such as Co, Ni, and Cu, highlighting the distinct preferential adsorption behavior of the resin.

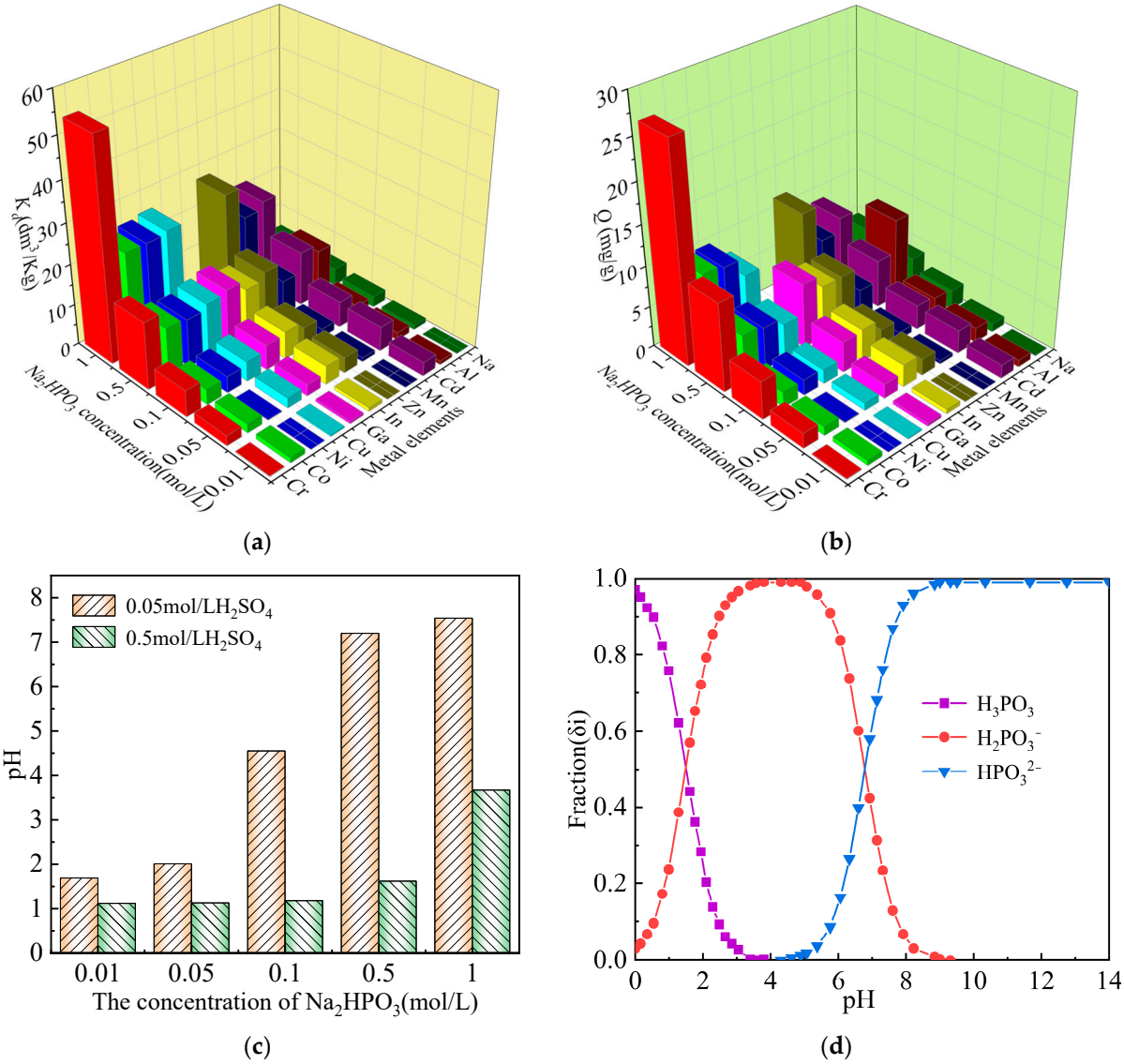


Figure 2. Effect of sodium phosphite concentration on ion adsorption by IRA-900 resin: (**a**) Distribution coefficient; (**b**) Adsorption capacity; (**c**) Solution pH; (**d**) The δi-pH of the Na_2HPO_3 solution (Adsorption time: 2 h, Temperature: 298 K, V/m: 10 mL/0.1 g).

The effect of sodium phosphite concentration on solution pH is shown in Figure 2c. The pH increased progressively with higher sodium phosphite concentrations, which can be attributed to the stronger hydrolysis tendency of HPO_3^{2-} compared to its ionization in acidic media [26]. Comparative analysis indicated that 0.5 mol·L^{-1} sulfuric acid provided better pH stabilization than 0.05 mol·L^{-1} sulfuric acid, effectively maintaining acidic conditions favorable for adsorption. At 1 mol·L^{-1} sodium phosphite (pH 3.5), the resin exhibited relatively high Cr^{3+} adsorption capacity; therefore, 0.5 mol·L^{-1} sulfuric acid was selected as the baseline condition for subsequent experiments. The speciation distribution of phosphite ions as a function of pH is illustrated in Figure 2(d). Three main phosphorus-containing species exist in sodium phosphite solutions: H_3PO_3, $H_2PO_3^-$, and HPO_3^{2-}. H_3PO_3 predominates at pH < 1.3, $H_2PO_3^-$ is the major species in the pH range of 1.3–6.9, and HPO_3^{2-} dominates at pH > 6.9 [27]. Under the selected conditions of 0.5 mol·L^{-1} H_2SO_4 and 1 mol·L^{-1} Na_2HPO_3 (pH 3.5), $H_2PO_3^-$ accounted for approximately 99% of the

species, suggesting that Cr^{3+} adsorption likely occurs through the formation of an anionic complex with $H_2PO_3^-$. Although IRA-900 is an anion-exchange resin, slight adsorption of transition metal cations (Co^{2+}, Ni^{2+}, Cu^{2+}) was observed in competitive adsorption experiments (Figure 2a). This can be explained by the formation of anionic metal–phosphite complexes, which are subsequently captured by the quaternary ammonium groups on the resin [28]. The low distribution coefficients (<20 $dm^3 \cdot kg^{-1}$) suggest that cation exchange or precipitation plays only a minor role. Consequently, in multicomponent simulated wastewater containing competing ions such as Co^{2+}, Ni^{2+}, and Cu^{2+}, the IRA-900 resin shows outstanding selectivity for Cr(III), with negligible co-adsorption of other metal ions. Such high selectivity is rare among conventional adsorbents and is particularly advantageous for treating actual industrial wastewater.

3.2. Effect of Sulfuric Acid Concentration

The influence of solution acidity on adsorption performance was systematically evaluated by measuring Cr^{3+} adsorption capacities at sulfuric acid concentrations of 0.5, 1, 2, and 3 $mol \cdot L^{-1}$ (Figure 3). In the absence of sodium phosphite, the resin showed negligible adsorption of Cr^{3+}. When 1 $mol \cdot L^{-1}$ sodium phosphite was introduced, the maximum Cr^{3+} adsorption capacity (14.9 $mg \cdot g^{-1}$) was achieved at 0.5 $mol \cdot L^{-1}$ H_2SO_4, with a progressive decrease observed as acid concentration increased. This trend can be explained by the speciation behavior of phosphite: under highly acidic conditions (pH < 1.3), H_3PO_3 becomes the dominant species. Since H_3PO_3 has a weaker complexation ability with Cr^{3+} compared to $H_2PO_3^-$, the adsorption efficiency is reduced [27].

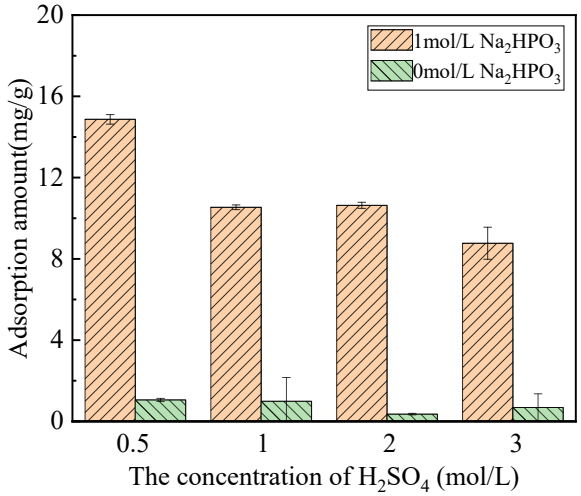


Figure 3. Effect of sulfuric acid concentration on Cr^{3+} adsorption capacity(Adsorption time: 2 h, Temperature: 298 K, V/m: 10 mL/0.1 g).

3.3. Effects of Time and Temperature

The adsorption kinetics and the effect of temperature on Cr^{3+} uptake are shown in Figure 4. The resin exhibited rapid adsorption, reaching 90% of its maximum capacity within 30 min. Subsequently, the adsorption rate gradually decreased, approaching equilibrium at 180 min with a capacity of 14.5 $mg \cdot g^{-1}$ at 318 K. Increasing the temperature from 298 K to 318 K not only raised the equilibrium adsorption capacity from 13.5 $mg \cdot g^{-1}$ to 14.5 $mg \cdot g^{-1}$ but also significantly accelerated the adsorption kinetics.

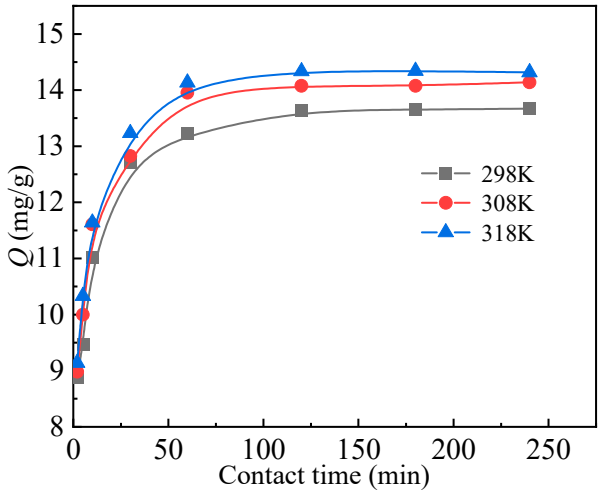


Figure 4. Effect of time and temperature on adsorption capacity(H_2SO_4: 0.5 mol/L, Na_2HPO_3: 1 mol/L, V/m: 10 mL/0.1 g).

3.4. Effect of Initial Ion Concentration of Cr(III)

The equilibrium adsorption capacity as a function of the initial Cr^{3+} concentration is shown in Figure 5. The adsorption capacity increased progressively from 5.02 $mg \cdot g^{-1}$ to 60.13 $mg \cdot g^{-1}$ as the initial concentration rose from 20 $mg \cdot L^{-1}$ to 400 $mg \cdot L^{-1}$, with specific values of 19.28 $mg \cdot g^{-1}$ at 100 $mg \cdot L^{-1}$ and 33.20 $mg \cdot g^{-1}$ at 200 $mg \cdot L^{-1}$. This trend is attributed to the stronger concentration gradient at higher Cr^{3+} levels, which enhances the mass transfer driving force and promotes adsorption [29]. Correspondingly, the adsorption kinetics accelerated with increasing initial concentration, although the time required to reach equilibrium extended from 10 min (at 20 $mg \cdot L^{-1}$) to 60 min (at 400 $mg \cdot L^{-1}$), with intermediate equilibration times of 20 min and 30 min observed at 100 $mg \cdot L^{-1}$ and 200 $mg \cdot L^{-1}$, respectively. This pattern reflects the combined effects of concentration-driven adsorption enhancement and intraparticle diffusion limitations.

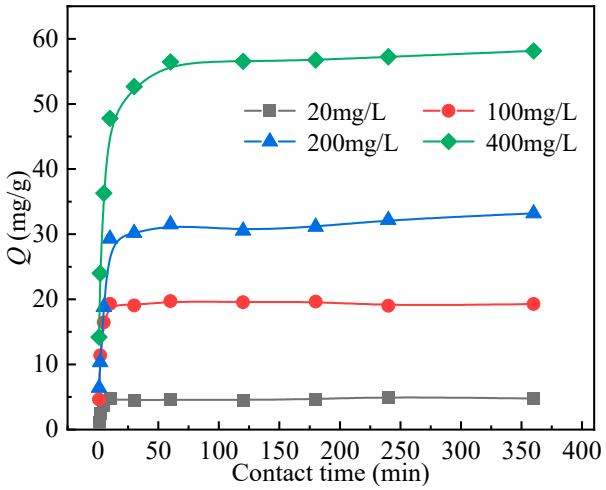


Figure 5. Effect of initial ion concentration and time on adsorption capacity(H_2SO_4: 0.5 mol/L, Na_2HPO_3: 1 mol/L, V/m: 20 mL/0.025 g).

In comparison with other adsorbents (Table of Section 3.8), the IRA-900 resin in this study achieved a high maximum adsorption capacity of 103.56 $mg \cdot g^{-1}$ at an initial concentration of 1000 $mg \cdot L^{-1}$. This performance exceeds that of several reported materials, such as SD-g-AAc (13.81 $mg \cdot g^{-1}$) and DETA-grafted Merrifield resin (38.35 $mg \cdot g^{-1}$), and is comparable to high-capacity adsorbents like EDTA-modified attapulgite (131.37 $mg \cdot g^{-1}$) and peanut shell-derived

adsorbent (104.82 mg·g^{-1}). More notably, alongside its high capacity, the proposed system offers exceptional selectivity and significant structural stability after adsorption—distinct advantages that are not commonly achieved by conventional adsorbents.

3.5. Adsorption Kinetics

The adsorption kinetics of Cr(III) were evaluated at three different temperatures (298, 308, and 318 K). The experimental data were fitted with three kinetic models: intraparticle diffusion, pseudo-first-order, and pseudo-second-order, as shown in Figure 6a–c and summarized in Table 2. Figure 6a presents two distinct linear regions in the intraparticle diffusion model, indicating multiple adsorption stages involving film diffusion, pore diffusion, and equilibrium. The slope k_p reflects the intraparticle diffusion rate, with higher values corresponding to faster adsorption. In the first stage, the k_p values at 298 K, 308 K, and 318 K were 0.8940, 0.8759, and 0.9195, respectively, suggesting that pore diffusion controls the initial adsorption and that the IRA-900 resin exhibits a high adsorption rate for Cr(III). The porous structure of the resin provides abundant active sites on its internal channels, facilitating rapid uptake [30]. In the second stage, adsorption gradually approaches equilibrium. Notably, the fitted lines at all temperatures do not pass through the origin, implying that the overall process involves both chemical adsorption (ion exchange) and intraparticle diffusion. According to Table 2, the pseudo-second-order model yields a correlation coefficient (R^2)of 0.9999, indicating an excellent fit. This supports that the adsorption follows pseudo-second-order kinetics, with chemical adsorption as the rate-limiting step. Therefore, in the Na_2HPO_3–H_2SO_4 system, ion exchange is the predominant adsorption mechanism.

Table 2. Kinetic parameters of the resin adsorption towards Cr(III) at 298, 308 and 318 K.

T (*K*)	PFO			PSO			Intra-Particle Diffusion		$Q_{e,\,exp}$ (mg/g)
	k_1 (min^{-1})	Q_e (mg/g)	R^2	k_2 (g/mg/min)	Q_e (mg/g)	R^2	k_p	R^2	
298	0.032	1.2795	0.9549	0.073	13.65	0.9999	0.8940	0.9882	13.67
308	0.026	1.0988	0.8544	0.070	14.08	0.9999	0.8758	0.9829	14.14
318	0.020	1.1437	0.8446	0.069	14.34	0.9999	0.9195	0.9931	14.32

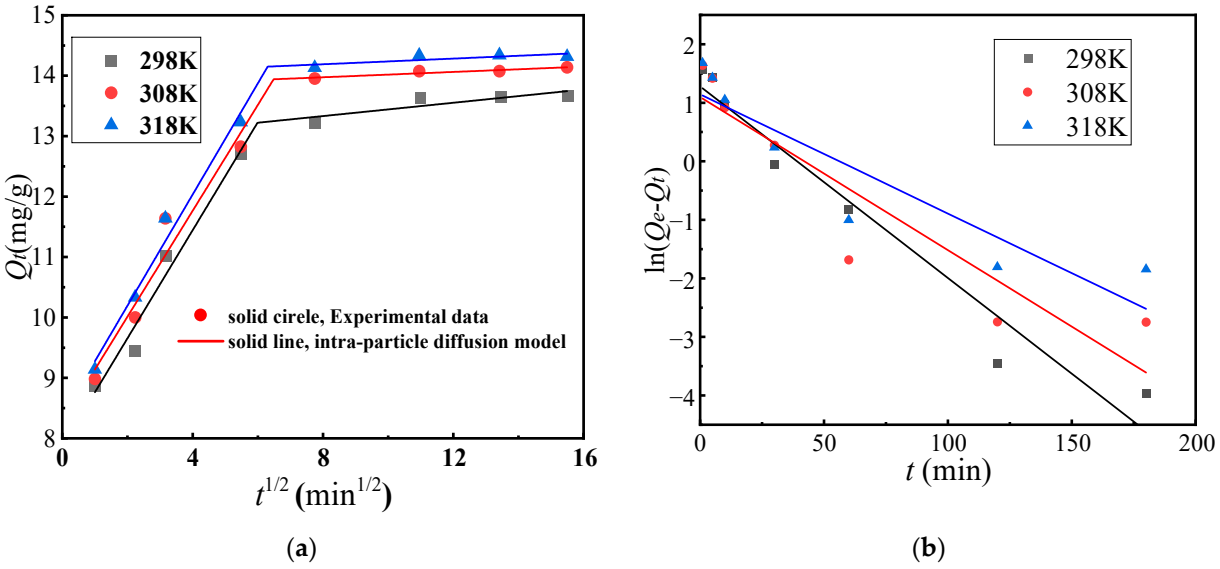
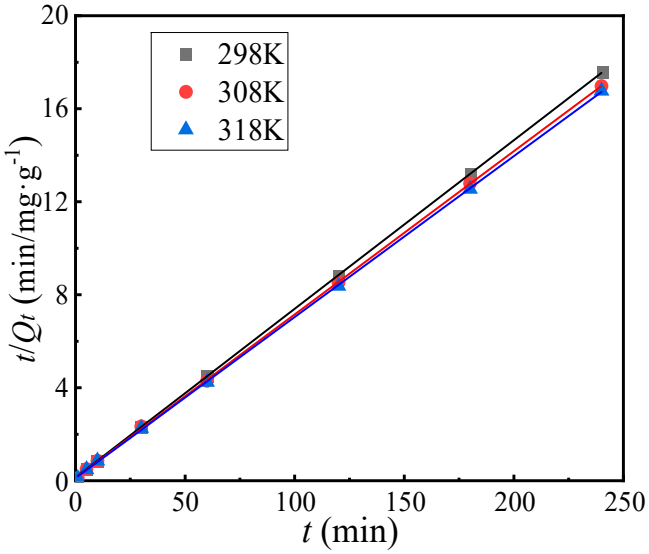


Figure 6. *Cont.*



(**c**)

Figure 6. (**a**) intra-particle diffusion model, (**b**) pseudo-first-order, (**c**) pseudo-second-order (H_2SO_4: 0.5 mol/L, Na_2HPO_3: 1 mol/L, V/m: 10 mL/0.1 g).

3.6. Adsorption Isotherms

The adsorption isotherms at varying temperatures were determined by systematically modulating the initial Cr^{3+} concentration and thermal conditions. Experimental data were analyzed through nonlinear regression using both Langmuir and Freundlich isotherm models. As illustrated in Figure 7 and quantified in Table 3, the equilibrium adsorption capacity increased progressively with the Cr^{3+} equilibrium concentration until saturation was reached. Elevated temperatures significantly improved adsorption performance, with the maximum uptake capacity reaching 103.56 mg·g^{-1} at 318 K under optimized conditions. Comparative analysis indicated that the Langmuir model provided a higher correlation coefficient (R^2 approaching unity), and its theoretical maximum adsorption capacity (Q_m) aligned more closely with experimental values than the Freundlich model. These results confirm that the adsorption of Cr^{3+} onto the IRA-900 resin follows the Langmuir model, indicating a monolayer adsorption process dominated by chemical interactions. Previous studies have also affirmed that the Langmuir model offers the best fit when adsorption is governed by specific homogeneous chemical mechanisms. For example, Song et al. [31], reported that the Langmuir model well described Cr(VI) adsorption on amine-functionalized adsorbents, which was attributed to coordination between amine groups and metal ions—a mechanism analogous to the ion exchange between quaternary ammonium groups and the Cr(III)–$H_2PO_3^-$ complex observed in this study.

Table 3. Adsorption isotherm parameters of Cr^{3+} on IRA-900.

T (*K*)	Langmuir Isotherm			Freundlich Isotherm			$Q_{e,exp}$ (mg/g)
	K_L ($\times 10^{-5}$) (L/mg)	Q_m (mg/g)	R^2	n	K_f (mg^{1-n}·L^n/g)	R^2	
298	4.00	99.88	0.994	2.17	3.82	0.905	97.9854
308	3.74	102.00	0.983	2.29	4.71	0.918	99.7563
318	4.06	104.76	0.984	2.36	5.36	0.917	103.562

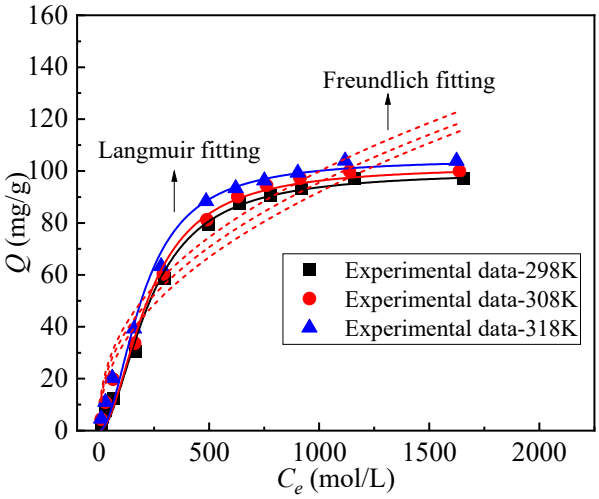


Figure 7. Adsorption isotherm on IRA-900 resin towards Cr^{3+} (H_2SO_4: 0.5 mol/L, Na_2HPO_3: 1 mol/L, Time: 24 h, Temperature: 298, 308, 318 K, V/m: 40 mL/0.05 g).

3.7. Desorption Experiments

Figure 8a presents the Cr^{3+} desorption performance of the IRA-900 resin under standardized conditions (298 K, 1 mol·L^{-1} desorbent concentration, liquid-to-solid ratio of 10 mL/0.01 g) using seven eluents: HNO_3, H_2SO_4, HCl, NaOH, NH_4Cl, NaCl, and $NH_3 \cdot H_2O$. The results indicate consistently low Cr^{3+} desorption efficiencies (<5%) across all eluents, reflecting the negligible release of adsorbed ions. This systematic evaluation underscores the strong retention of Cr^{3+} on the resin, consistent with dominant chemisorption interactions that resist conventional desorption.

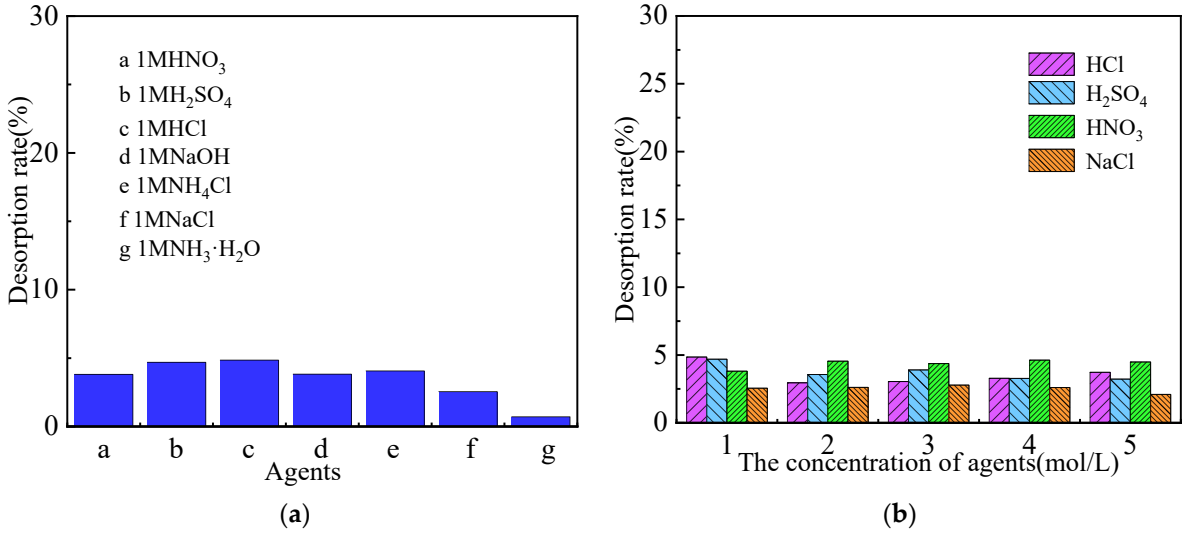


Figure 8. (**a**) Effect of different desorbent on the desorption rate of Cr^{3+}; (**b**) Effect of desorbent concentration on the desorption rate of Cr^{3+} (The resin used for desorption was saturated under the following adsorption conditions: 1000 ppm Cr(III), V/m: 40 mL/0.05 g, 1 mol/L Na_2HPO_3, duration of 24 h, temperature of 298 K, and 0.5 mol/L H_2SO_4).

Figure 8b shows the effect of desorbent concentration (1–5 mol·L^{-1}) on Cr^{3+} desorption efficiency under fixed conditions (298 K, liquid-to-solid ratio of 10 mL/0.01 g). Four desorbents were tested, yet the Cr^{3+} desorption rate remained below 5% across all concentrations. The absence of improvement with increasing desorbent concentration confirms that Cr^{3+} cannot be effectively eluted, suggesting the formation of a highly stable Cr–resin complex. These results demonstrate that conventional desorbents fail to remove

Cr^{3+} from the resin, highlighting the strong binding affinity within the resin matrix [32]. This behavior is attributed to the dominant chemisorption interaction and the high stability of the Cr(III)–phosphite complex formed on the resin, which remains intact even under exposure to typical eluents. The resin structure remains stable after adsorption, and Cr(III) resists desorption by common reagents such as acids, alkalis, and salts. This property provides a new pathway for the solidification treatment of Cr(III), effectively preventing secondary pollution and showing potential advantages in environmental safety. Future studies may focus on either (1) developing more effective eluents for Cr(III) recovery or (2) utilizing the resin for direct Cr(III) immobilization to reduce environmental risks from Cr(III)-containing wastewater.

3.8. Comparison with Reported Adsorbents

Table 4 presents the comparative adsorption performance of different adsorbents toward Cr(III). It can be observed that most adsorbents require a higher dosage to achieve satisfactory adsorption efficiency compared with the IRA-900 resin, indicating the superior adsorption capability of sodium phosphite-treated IRA-900 resin for chromium-containing wastewater. Furthermore, the IRA-900 resin exhibits excellent structural stability after chromium adsorption, showing minimal desorption in both acidic and alkaline solutions. Several existing adsorbents (e.g., chitosan, peanut shell-derived adsorbents) exhibit relatively high adsorption capacities. However, the IRA-900 resin used in this study demonstrates distinct advantages in terms of selectivity, stability, and operational simplicity. In particular, it maintains efficient adsorption under acidic conditions, thus avoiding the performance degradation observed with most biomass-based adsorbents at low pH.

Table 4. Comparison of reported adsorbents for Cr(III) in the literature with the present study.

Materials	Adsorbent Dosage	Initial Ion Concentration	Q_m (mg·g^{-1})	Ref.
Sodium phosphite and IRA-900 resin	0.05 g/40 mL	1000 ppm	103.56	This study
SD-g-AAc(gamma irradiated acrylic acid-grafted-sawdust)	2 g/50 mL	800 ppm	13.81	[33]
Chitosan flakes	0.5 g/50 mL	2000 ppm	138.45	[34]
Leonardite	0.5 g/500 mL	500 ppm	75.2	[35]
DETA grafted Merrifield resin	0.15 g/20 mL	300 ppm	38.35	[36]
EDTA modified attapulgite	0.02 g/50 mL	120 ppm	131.37	[37]
adsorbent from peanut shell (PNS)	2.5 g/1000 mL	363 ppm	104.82	[38]

3.9. Investigation of Adsorption Mechanism

XPS analysis was performed on sodium phosphite and the resin before and after adsorption, as shown in Figure 9a. The high-resolution narrow spectra of Cr2p and P2p for the resin after adsorption are presented in Figure 9b,c, respectively. In the sodium phosphite spectrum, characteristic peaks of P2p, O1s, and Na1s were observed, consistent with the elemental composition of sodium phosphite. Compared to the resin before adsorption, the post-adsorption resin exhibited a characteristic P2p peak with a binding energy increase from 131.5 eV to 132.77 eV [39], along with a significant enhancement of the O1s peak at 531.2 eV, which may be attributed to the coordination between HPO_3^{2-} and Cr. A characteristic Cr peak appeared at 552.8 eV, confirming the successful adsorption of Cr. In the narrow spectra of Cr2p and P2p, the characteristic peaks for Cr2p3/2 and Cr2p1/2 orbitals were observed at 577.51 eV and 587.11 eV, respectively [40], while the P2p peak appeared at 132.77 eV.

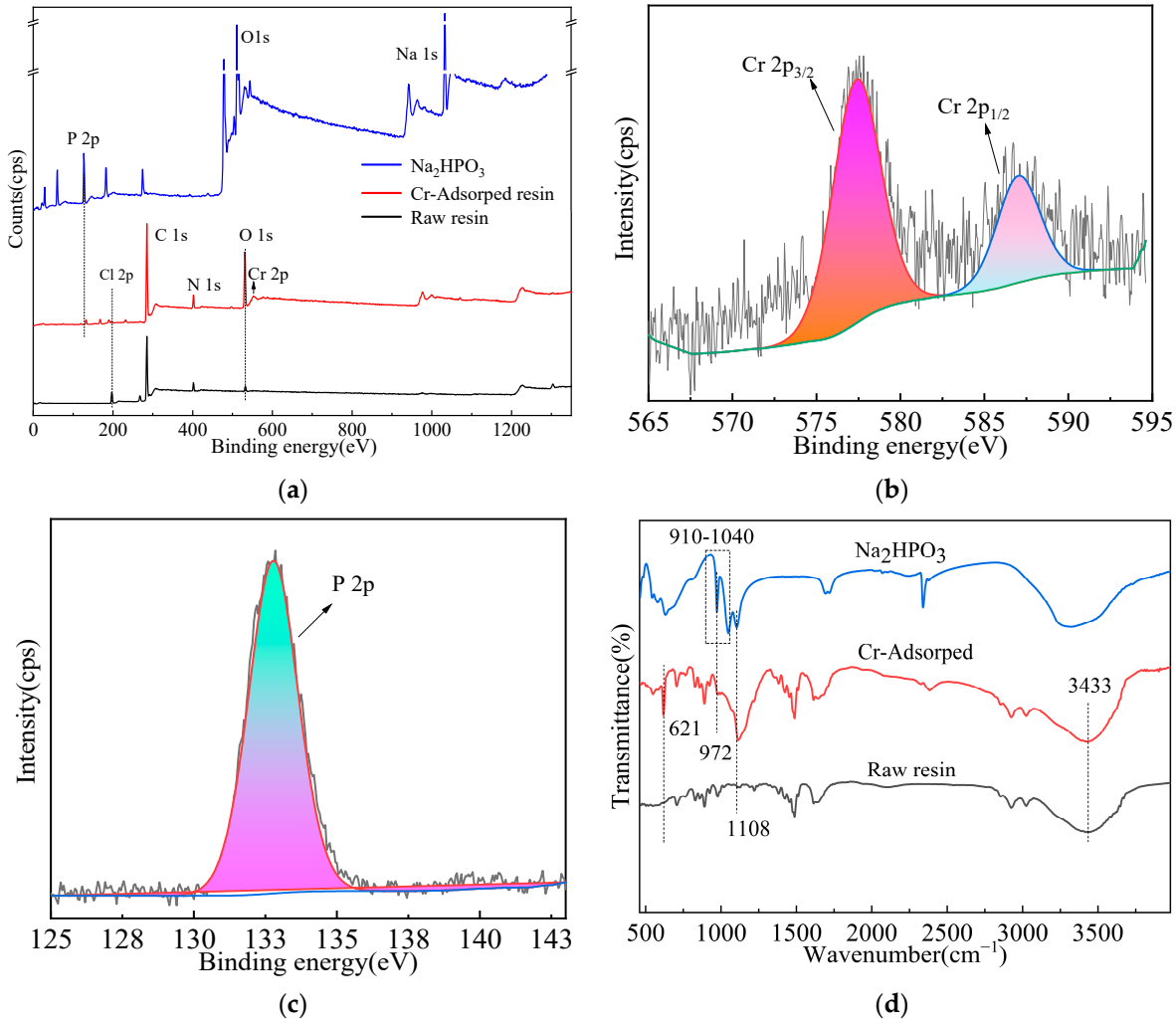


Figure 9. (**a**) Full XPS spectrum of the resin and Na_2HPO_3; (**b**) narrow XPS spectrum of Cr2p; (**c**) narrow XPS spectrum of P2p; (**d**) FT-IR spectra of resin and Na_2HPO_3.

The FT-IR spectra of the resin and Na_2HPO_3 are shown in Figure 9d. In the infrared spectra of the resin before and after adsorption, the characteristic -OH peak appeared at 3433 cm^{-1}, attributed to water entrapped in the resin during adsorption or from ambient air [41]. In the sodium phosphite spectrum, the asymmetric stretching vibration of P=O was observed at 1108 cm^{-1}, the symmetric stretching vibration of P=O at 972 cm^{-1}, and the P-OH stretching vibration band appeared between 1040 and 910 cm^{-1}, which complicates the infrared spectrum of hydrogen phosphate compounds in the phosphorus-oxygen stretching vibration region. In the spectrum of the resin after Cr^{3+} adsorption, distinct asymmetric and symmetric P=O stretching vibration peaks were observed, but their positions shifted significantly from 1108 cm^{-1} and 972 cm^{-1} to 1115 cm^{-1} and 977 cm^{-1}, respectively [42], likely due to coordination with Cr^{3+}. Additionally, a prominent vibration peak emerged at 621 cm^{-1} in the Cr^{3+}-adsorbed resin, which may be associated with the adsorption of Cr^{3+}.

The SEM-EDS spectra of the resin before and after adsorption are shown in Figure 10. The primary elements of the pristine resin were C, N, and Cl. After adsorption, additional elements (P, O, and Cr) were detected in the resin, confirming the successful adsorption of Cr^{3+}.

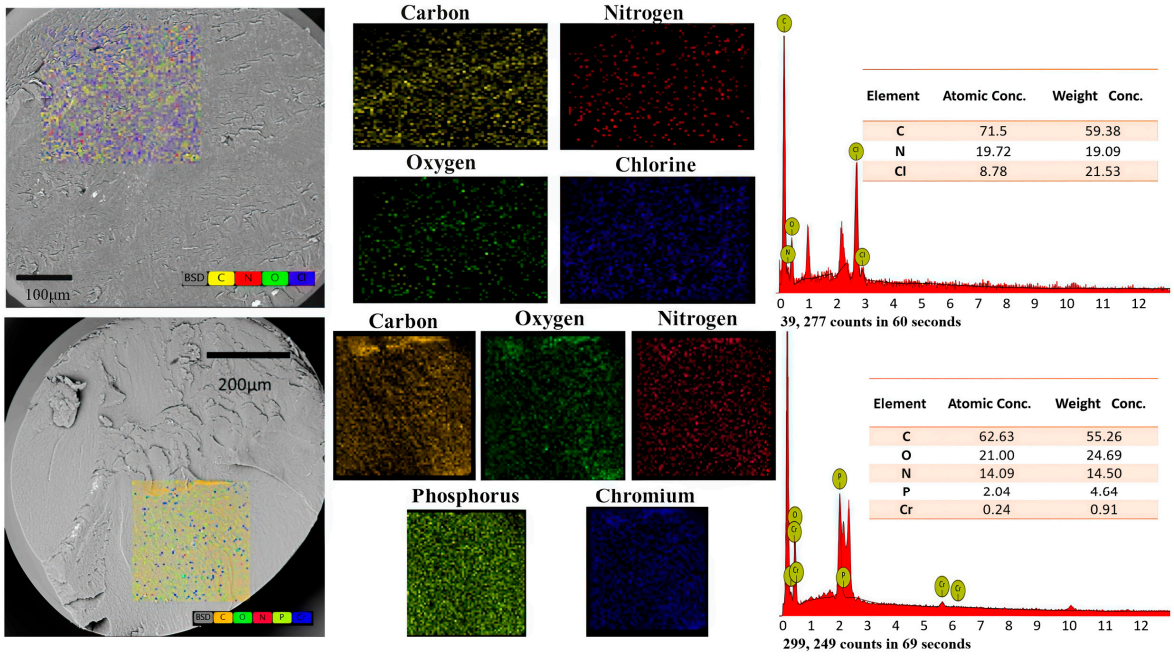


Figure 10. The SEM-EDS of resin before and after adsorption.

The proposed adsorption mechanism involves a two-step process. First, in the H_2SO_4-Na_2HPO_3 system, Cr^{3+} ions coordinate with the dominant $H_2PO_3^-$ species to form negatively charged anionic complexes, such as $[Cr(H_2PO_3)_n]^{(3-n)}$ (where n > 4). Subsequently, these Cr(III)-containing anionic complexes are attracted to the positively charged quaternary ammonium groups ($-N^+R_3$) on the IRA-900 resin via electrostatic interactions. This is followed by an ion-exchange process where the Cr(III)-containing anionic complexes displace the original Cl^- counterions on the functional groups, thus becoming firmly fixed onto the resin. The formation of the Cr–P coordination bonds is confirmed by the peak shifts in XPS and FT-IR analyses, while the decrease in Cl content on the resin (EDS) provides direct evidence for the ion-exchange step. This combination of complexation and ion exchange explains the high selectivity and strong stability of Cr(III) on the resin.

4. Conclusions

This study proposes and validates, for the first time, the selective adsorption of Cr(III) by IRA-900 resin via a ligand-assisted anion-exchange mechanism in a sodium phosphite–sulfuric acid system. Cr(III) forms a negatively charged complex with $H_2PO_3^-$, which subsequently undergoes electrostatic interaction and ion exchange with the quaternary ammonium groups on the resin. This mechanism differs from traditional cation adsorption or physical adsorption, providing a novel approach for the highly selective removal of Cr(III).

(1) In the sodium phosphite-sulfuric acid system, IRA-900 resin exhibited favorable adsorption performance for Cr, with minor adsorption of other elements. At a sodium phosphite concentration of 1 $mol \cdot L^{-1}$, the distribution coefficient and adsorption capacity of the resin for Cr^{3+} reached 55 $dm^3 \cdot kg^{-1}$ and 27 $mg \cdot g^{-1}$, respectively, achieving adsorption equilibrium within 180 min.

(2) The maximum adsorption capacity was 103.56 $mg \cdot g^{-1}$. The adsorption process followed the Langmuir isothermal model more closely, indicating monolayer chemisorption. The structure of Cr^{3+}-adsorbed IRA-900 resin demonstrated strong stability, making Cr^{3+} difficult to desorb using conventional eluents. Subsequent research should focus on either (1) identifying a more effective desorbent for Cr(III) removal or (2) exploring

the immobilization of Cr(III) on IRA-900 resin to minimize environmental pollution from Cr(III)-containing wastewater.

(3) XPS/FT-IR/SEM-EDS analyses revealed that the adsorption mechanism likely involves the coordination of Cr^{3+} with $H_2PO_3^-$ to form an anionic complex, which subsequently undergoes ion exchange with Cl^- on the resin.

(4) Processes based on ion-exchange resins are already well-established in industrial water treatment and possess significant potential for scale-up. The use of sodium phosphite represents a key cost factor in this study for achieving high selectivity. Future economic assessments will need to balance its consumption against the savings in hazardous waste treatment costs and potential product value. Furthermore, residual phosphite after adsorption can be removed by the following methods: ① adjusting the pH to alkaline conditions (pH > 8) to facilitate phosphite removal via precipitation; ② oxidative treatment (e.g., using hydrogen peroxide) to convert phosphite into phosphate. Phosphate is bioavailable to plants and exhibits significantly lower ecotoxicity compared to chromium.

This study not only proposes a novel adsorption system for Cr(III) but also demonstrates its achievement of high selectivity through ligand assistance, along with excellent stability and solidification potential. This strategy provides a new technical pathway for the resource recovery and harmless treatment of chromium-containing wastewater, exhibiting certain scientific significance and practical application value.

Author Contributions: Conceptualization, C.H.; methodology, C.H., T.X.; validation, C.H., T.X.; formal analysis, T.X., D.G.; investigation, T.X., D.G.; data curation, Y.Y. and G.W. and Q.W.; writing—original draft preparation, T.X. and Y.Y.; writing—review and editing, C.H., G.W. and T.X.; supervision, C.H. and Q.W.; project administration, C.H. and G.W.; funding acquisition, C.H. and Q.W. All authors have read and agreed to the published version of the manuscript.

Funding: This project was funded by the Natural Science Foundation of Guangxi Province, China, grant number 2024GXNSFAA010485, Central Funds Project for Guiding Local Technological Development (ZY24212006), the Special Fund for Science and Technology Development of Guangxi, grant number AD25069078, and the Natural Science Foundation of China, grant number 52364022.

Data Availability Statement: Data are contained within the article.

Conflicts of Interest: The authors declare no conflicts of interest.

Abbreviations

The following abbreviations are used in this manuscript:

DETA	Diethylenetriamine
EDTA	Ethylene Diamine Tetraacetic Acid

References

1. Zhao, P.; Zhang, H.; Yu, J.; Gao, H.; Cao, Y.; Zhu, Y.; Zhao, H. Conditions for mutual conversion of Cr(III) and Cr(VI) in aluminum chromium slag. *J. Alloys Compd.* **2019**, *788*, 506–513. [CrossRef]
2. Kapoor, R.T.; Mfarrej, M.F.B.; Alam, P.; Rinklebe, J.; Ahmad, P. Accumulation of chromium in plants and its repercussion in animals and humans. *Environ. Pollut.* **2022**, *301*, 119044. [CrossRef] [PubMed]
3. Coetzee, J.J.; Bansal, N.; Chirwa, E.M. Chromium in environment, its toxic effect from chromite-mining and ferrochrome industries, and its possible bioremediation. *Expo. Health* **2018**, *12*, 51–62. [CrossRef]
4. Mortada, W.I.; El-Naggar, A.; Mosa, A.; Palansooriya, K.N.; Yousaf, B.; Tang, R.; Wang, S.; Cai, Y.; Chang, S.X. Biogeochemical behaviour and toxicology of chromium in the soil-water-human nexus: A review. *Chemosphere* **2023**, *331*, 138804. [CrossRef]
5. Mortazavian, S.; An, H.; Chun, D.; Moon, J. Activated carbon impregnated by zero-valent iron nanoparticles (AC/nZVI) optimized for simultaneous adsorption and reduction of aqueous hexavalent chromium: Material characterizations and kinetic studies. *Chem. Eng. J.* **2018**, *353*, 781–795. [CrossRef]

6. Lyu, H.; Tang, J.; Huang, Y.; Gai, L.; Zeng, E.Y.; Liber, K.; Gong, Y. Removal of hexavalent chromium from aqueous solutions by a novel biochar supported nanoscale iron sulfide composite. *Chem. Eng. J.* **2017**, *322*, 516–524. [CrossRef]
7. Sughis, M.; Nawrot, T.S.; Haufroid, V.; Nemery, B. Adverse health effects of child labor: High exposure to chromium and oxidative DNA damage in children manufacturing surgical instruments. *Environ. Health Perspect.* **2012**, *120*, 1469–1474. [CrossRef]
8. Dhal, B.; Thatoi, H.; Das, N.; Pandey, B. Chemical and microbial remediation of hexavalent chromium from contaminated soil and mining/metallurgical solid waste: A review. *J. Hazard. Mater.* **2013**, *250*, 272–291. [CrossRef]
9. Ma, H.; Hua, L.; Lian, K.; Ma, X. Adsorptive removal of trivalent chromium in aqueous solution using precipitate produced from aluminum tanning wastewater. *Water Air Soil Poll.* **2014**, *225*, 1956. [CrossRef]
10. Ajiboye, T.O.; Oyewo, O.A.; Onwudiwe, D.C. Simultaneous removal of organics and heavy metals from industrial wastewater: A review. *Chemosphere* **2021**, *262*, 128379. [CrossRef]
11. Zha, S.; Yu, A.; Wang, Z.; Shi, Q.; Cheng, X.; Liu, C.; Deng, C.; Zeng, G.; Luo, S.; Zhao, Z. Microbial strategies for effective hexavalent chromium removal: A comprehensive review. *Chem. Eng. J.* **2024**, *489*, 151457. [CrossRef]
12. Ukhurebor, K.E.; Aigbe, U.O.; Onyancha, R.B.; Nwankwo, W.; Osibote, O.A.; Paumo, H.K.; Ama, O.M.; Adetunji, C.O.; Siloko, I.U. Effect of hexavalent chromium on the environment and removal techniques: A review. *J. Environ. Manag.* **2021**, *280*, 111809. [CrossRef]
13. Mitra, S.; Sarkar, A.; Sen, S. Removal of chromium from industrial effluents using nanotechnology: A review. *Nanotechnol. Environ. Eng.* **2017**, *2*, 11. [CrossRef]
14. Acharya, R.; Sillanpää, M.; Al-Farraj, S. A comprehensive review on sequestration of aqueous Cr(VI) over graphene based adsorbents. *J. Hazard. Mater. Adv.* **2025**, *18*, 100670. [CrossRef]
15. Jiao, F.; Li, W.; Xue, K.; Yang, C.; Qin, W. Recovery of chromium and magnesium from spent magnesia-chrome refractories by acid leaching combined with alkali precipitation and evaporation. *Sep. Purif. Technol.* **2019**, *227*, 115705. [CrossRef]
16. Yao, F.; Jia, M.; Yang, Q.; Luo, K.; Chen, F.; Zhong, Y.; He, L.; Pi, Z.; Hou, K.; Wang, D. Electrochemical Cr (VI) removal from aqueous media using titanium as anode: Simultaneous indirect electrochemical reduction of Cr (VI) and in-situ precipitation of Cr (III). *Chemosphere* **2020**, *260*, 127537. [CrossRef]
17. Da Silva, G.; Dos Santos, F.; Roth, G.; Frankenberg, C. Electroplating for chromium removal from tannery wastewater. *Int. J. Environ. Sci. Technol.* **2020**, *17*, 607–614. [CrossRef]
18. Riaz, T.; Ahmad, A.; Saleemi, S.; Adrees, M.; Jamshed, F.; Hai, A.M.; Jamil, T. Synthesis and characterization of polyurethane-cellulose acetate blend membrane for chromium (VI) removal. *Carbohydr. Polym.* **2016**, *153*, 582–591. [CrossRef]
19. Wang, Y.; Liu, Y.; Meng, F.; Zhang, J.; Zhao, S.; Tian, X.; Wang, L.; Chen, D.; Qi, T. Efficient separation of vanadium and chromium by the complexation with sulfate ions in solvent extraction using EHEHPA. *Sep. Purif. Technol.* **2025**, *354*, 129281. [CrossRef]
20. Rim, S.A.; Amine, D.M.; Nasr-Eddine, B.; Canselier, J.P. Removal of chromium (III) by two-aqueous phases extraction. *J. Hazard. Mater.* **2009**, *167*, 896–903. [CrossRef]
21. Elabbas, S.; Mandi, L.; Berrekhis, F.; Pons, M.N.; Leclerc, J.P.; Ouazzani, N. Removal of Cr (III) from chrome tanning wastewater by adsorption using two natural carbonaceous materials: Eggshell and powdered marble. *J. Environ. Manage.* **2016**, *166*, 589–595. [CrossRef]
22. Fu, D.; Wang, G.; Zhao, L.; Hong, Y.; Yang, B.; Cheng, H. Design of ion-imprinted amino-modified chitosan for selective chromium (III) ion removal. *Sep. Purif. Technol.* **2024**, *336*, 126341. [CrossRef]
23. Elwakeel, K.; Elgarahy, A.; Elshoubaky, G.; Mohammad, S. Microwave assist sorption of crystal violet and Congo red dyes onto amphoteric sorbent based on upcycled Sepia shells. *J. Environ. Health Sci. Eng.* **2020**, *18*, 35–50. [CrossRef]
24. Fabbricino, M.; Naviglio, B.; Tortora, G.; d'Antonio, L. An environmental friendly cycle for Cr (III) removal and recovery from tannery wastewater. *J. Environ. Manag.* **2013**, *117*, 1–6. [CrossRef]
25. Aroua, M.K.; Zuki, F.M.; Sulaiman, N.M. Removal of chromium ions from aqueous solutions by polymer-enhanced ultrafiltration. *J. Hazard. Mater.* **2007**, *147*, 752–758. [CrossRef] [PubMed]
26. Truzzi, D.R.; Franco, D.W. Stability of phosphite coordinated to ruthenium (II) in aqueous media. *Polyhedron* **2014**, *81*, 238–244. [CrossRef]
27. Gally, C.; García-Gabaldón, M.; Ortega, E.; Bernardes, A.; Pérez-Herranz, V. Chronopotentiometric study of the transport of phosphoric acid anions through an anion-exchange membrane under different pH values. *Sep. Purif. Technol.* **2020**, *238*, 116421. [CrossRef]
28. Menezes, P.W.; Panda, C.; Loos, S.; Bunschei-Bruns, F.; Walter, C.; Schwarze, M.; Deng, X.; Dau, H.; Driess, M. A structurally versatile nickel phosphite acting as a robust bifunctional electrocatalyst for overall water splitting. *Energy Environ. Sci.* **2018**, *11*, 1287–1298. [CrossRef]
29. Zheng, C.; He, C.; Yang, Y.; Fujita, T.; Wang, G.; Yang, W. Characterization of waste amidoxime chelating resin and its reutilization performance in adsorption of Pb(II), Cu(II), Cd(II) and Zn(II) Ions. *Metals* **2022**, *12*, 149. [CrossRef]
30. Abu, A.; Abdullah, N. Sorption and thermodynamic study of nitrate removal by using Amberlite IRA 900 (AI900) resin. *Mater. Today Proc.* **2021**, *41*, 102–108. [CrossRef]

31. Song, Z.; Guo, K.; Bai, W.; Tang, C. Adsorption and removal of Cr (VI) from aqueous solution with amine-functionalized porous boron nitride. *J. Solid State Chem.* **2023**, *317*, 123720. [CrossRef]
32. Han, S.; Zang, Y.; Gao, Y.; Yue, Q.; Zhang, P.; Kong, W.; Jin, B.; Xu, X.; Gao, B. Co-monomer polymer anion exchange resin for removing Cr (VI) contaminants: Adsorption kinetics, mechanism and performance. *Sci. Total Environ.* **2020**, *709*, 136002. [CrossRef] [PubMed]
33. Ahmed, S.; Shahriar, A.; Rahman, N.; Alam, M.Z.; Nurnabi, M. Synthesis of gamma irradiated acrylic acid-grafted-sawdust (SD-g-AAc) for trivalent chromium adsorption from aqueous solution. *J. Hazard. Mater. Adv.* **2024**, *14*, 100427. [CrossRef]
34. Pietrelli, L.; Francolini, I.; Piozzi, A.; Sighicelli, M.; Silvestro, I.; Vocciante, M. Chromium (III) removal from wastewater by chitosan flakes. *Appl. Sci.* **2020**, *10*, 1925. [CrossRef]
35. Lao-Luque, C.; Solé, M.; Gamisans, X.; Valderrama, C.; Dorado, A.D. Characterization of chromium (III) removal from aqueous solutions by an immature coal (leonardite). Toward a better understanding of the phenomena involved. *Clean Technol. Environ. Policy* **2014**, *16*, 127–136. [CrossRef]
36. Bahsaine, K.; Mekhzoum, M.E.M.; Benzeid, H.; Qaiss, A.e.k.; Bouhfid, R. Chromium (III) adsorption from the phosphoric acid medium using DETA grafted Merrifield resin. *Environ. Sci. Pollut. Res.* **2023**, *30*, 67720–67729. [CrossRef]
37. Wang, J.; Zhang, D.; Liu, S.; Wang, C. Enhanced removal of chromium (III) for aqueous solution by EDTA modified attapulgite: Adsorption performance and mechanism. *Sci. Total Environ.* **2020**, *720*, 137391. [CrossRef] [PubMed]
38. Ahmed, S.; Sultana, R.; Nurnabi, M.; Alam, M.Z. Removal of Cr (III) from tanning effluent using adsorbent prepared from peanut shell. *Desalin. Water Treat.* **2022**, *266*, 91–100. [CrossRef]
39. Erçarıkcı, E.; Topcu, E.; Kıranşan, K.D. Flexible supercapacitor electrodes based on modified binary metal phosphites on three dimensional graphene sponge. *J. Alloys Compd.* **2023**, *930*, 167305. [CrossRef]
40. Song, Y.; Li, Z.; Shao, S.; Jiao, W.; Liu, Y. High-gravity intensified preparation of D201 resin-hydrated iron oxide nanocomposites for Cr (VI) removal. *Adv. Powder Technol.* **2021**, *32*, 1584–1593. [CrossRef]
41. Mohamed, H.S.; Soliman, N.; Abdelrheem, D.A.; Ramadan, A.A.; Elghandour, A.H.; Ahmed, S.A. Adsorption of Cd^{2+} and Cr^{3+} ions from aqueous solutions by using residue of Padina gymnospora waste as promising low-cost adsorbent. *Heliyon* **2019**, *5*, e01287. [CrossRef] [PubMed]
42. Zhao, R.; Hu, Y.; Ding, W.; Ren, K.; Gou, X.; Zhao, C.; Zheng, H. Simultaneous oxidation and adsorption of phosphite by magnetic $La_2(CO_3)_3/CoFe_2O_4$/biochar composite with peroxymonosulfate. *Chem. Eng. J.* **2023**, *451*, 138918. [CrossRef]

Disclaimer/Publisher's Note: The statements, opinions and data contained in all publications are solely those of the individual author(s) and contributor(s) and not of MDPI and/or the editor(s). MDPI and/or the editor(s) disclaim responsibility for any injury to people or property resulting from any ideas, methods, instructions or products referred to in the content.